THE JOURNAL OF PHYSICAL CHEMISTRY B

Article

pubs.acs.org/JPCB

# Molecular Mechanism of Specific Ion Interactions between Alkali Cations and Acetate Anion in Aqueous Solution: A Molecular Dynamics Study

Harsha V. R. Annapureddy and Liem X. Dang*

Chemical and Materials Sciences Division, Pacific Northwest National Laboratory, Richland, Washington 99352, United States

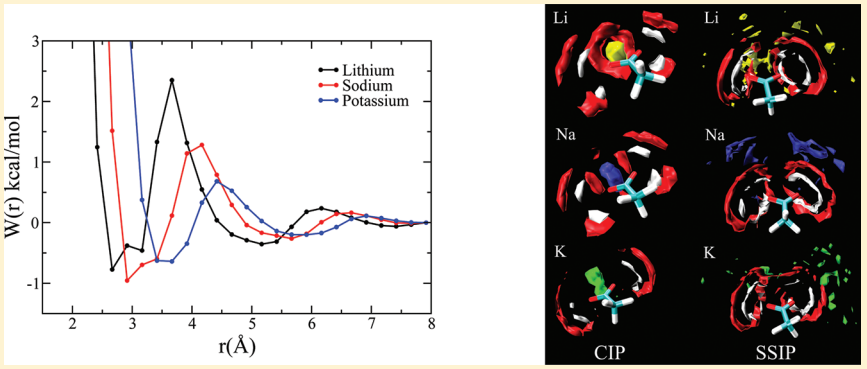


**ABSTRACT:** Specific ion interactions between alkali cations (i.e., $Li^+$, $Na^+$, and $K^+$) and an acetate anion in aqueous solution were studied using molecular dynamics simulation techniques and polarizable potential models. The ions−acetate systems were used as a model for understanding the interactions between ions and protein surfaces. We computed free energy profiles for different ion pairs using constrained mean force methods. Upon analyzing the computed free energy profiles for the $Na^+/K^+$−acetate ion-pairs, we observed a deeper contact ion minimum and also a larger association constant for the $Na^+$−acetate pair as compared to the corresponding $K^+$−acetate pair. These observations help to demonstrate the preferential binding of $Na^+$ over $K^+$ to protein surfaces. We also applied various rate theories to study the kinetics of ion pair interconversion.

## I. INTRODUCTION

Ion selectivity is vital in various chemical and biological processes. It has been reported that ion specificity influences protein interactions, enzymatic activity, and surface tension.[1−10] Since Hofmeister's discovery[11] of the ability of salts to precipitate proteins, there has been growing interest in understanding the effects of ion specificity. Through various studies, ions are ranked into a Hofmeister's series based on their degree of influence on the ability to precipitate proteins. The ions are classified into kosmotropes and chaotropes on the basis of their ability to alter the hydrogen-bonding network of water. Kosmotropes, which are referred to as water structure makers, are strongly hydrated and exhibit an effect known as "salting-out", which means they cause proteins to precipitate, while chaotropes are referred to as water structure breakers and exhibit a "salting-in" effect, which means they enhance protein solubility. This theory of bulk water structure making and breaking has been challenged by several experiments[12−16] and simulations.[17] Spectroscopic studies of Bakker and co-workers demonstrated that the ions of Hofmeister's series do not show a significant influence on the bulk water dynamics.[12−14] Pressure perturbation calorimetric measurements conducted by Pielak and co-workers also revealed no correlation between the specific ion effects and their impact on water structure.[16] These experiments clearly establish the fact that to understand the mechanism of Hofmeister's series, one need to consider the direct interactions between the ions and macromolecules.

Several studies have focused on advancing the understanding of ion specificity on protein surfaces. $Na^+$ and $K^+$ are the most abundant monovalent ions in biological systems. The concentration ratio of $Na^+$ to $K^+$ in the extracellular and intracellular regions is important in various biological processes. Jungwirth and co-workers reported that, because of the balance between the interactions of the ion with carboxylate groups and water, $Na^+$ has a greater affinity to a protein surface than does $K^+$.[7,18] Moreover, data from X-ray absorption spectroscopy (XAS) studies performed by Saykally and co-workers supported the understanding that $Na^+$ has a greater affinity for carboxylate anions than does $K^+$.[19] Their XAS spectra focused on C1s transition revealed that the binding affinity of alkali cations with carboxylate anions (i.e., acetate, formate, etc.) is of the order $Li^+ > Na^+ > K^+$. Another XAS study performed by Winter and co-workers focused on O1s transition showed a binding-affinity order of $Na^+ > Li^+ > K^+$, which is different from the order reported by Saykally and co-workers.[20] In our work, we used potential of mean force (PMF) calculations to provide

**Received:** February 24, 2012
**Revised:** May 31, 2012
**Published:** June 4, 2012

molecular-level details on specific ion interactions between alkali cations and acetate anions. Through the computed PMFs, we investigated the role of solvent effects along the reaction coordinate. We computed the binding free energies by integrating over the PMFs. We also investigated the kinetics of ion pair interconversion using various rate theories. In addition, the many-body effects were taken into account with the use of polarizable potential models.

## II. SIMULATION METHODS

In this study, polarizable models were used for all of the molecular-dynamics (MD) simulations. Parameters for $H_2O$, $Li^+$, $Na^+$, and $K^+$ were taken from our previous work.[21] For the acetate anion, the initial parameters were obtained from the general AMBER force field (GAFF).[22,23] Charges for the acetate anion were obtained from an ab initio RESP-fit at the Hartree−Fock(HF)/6-311+G* theory level using the Gaussian 98 program.[24] The original Lennard-Jones parameters from GAFF were adjusted slightly so the solvation enthalpy calculated from our simulations would match those obtained experimentally. All MD simulations were performed using a modified AMBER9 software package.[25] To obtain appropriate parameters that reproduce the solvation enthalpy for the acetate anion obtained experimentally,[26] we performed several molecular-dynamics simulations of an acetate ion solvated with 759 water molecules. These simulations were performed in a constant NPT ensemble at a temperature of 298 K and 1 bar pressure. The potential parameters are given in Table 1.

**Table 1. Potential Parameters for Water, Acetate, and Alkali Ions[a]**

| | atom type | $r^*$ (Å) | $\varepsilon$ (kcal/mol) | $q$ | $\alpha$ (Å$^3$) |
|---|---|---|---|---|---|
| acetate | CT | 4.3884 | 0.1094 | −0.4090 | 0.878 |
| | C | 4.3884 | 0.0860 | +1.1380 | 0.616 |
| | O | 3.8208 | 0.2100 | −0.9440 | 0.434 |
| | H | 3.4202 | 0.0157 | +0.0530 | 0.135 |
| alkali cations | $Na^+$ | 2.5400 | 0.1000 | +1.0000 | 0.240 |
| | $K^+$ | 3.4000 | 0.1000 | +1.0000 | 0.830 |
| | $Li^+$ | 1.7600 | 0.1000 | +1.0000 | 0.029 |
| water | OW | 3.6160 | 0.1825 | 0.0000 | 0.000 |
| | HW | 0.0000 | 0.0000 | +0.5190 | 0.000 |
| | M | 0.0000 | 0.0000 | −1.038 | 1.444 |

[a]CT is the carbon atom in methyl group, and C is the carbon bonded to oxygen atoms.

We employed a constrained molecular-dynamics methodology to evaluate the PMF for ion association.[27,28] In this calculation, the center of mass separation between the ions was chosen as a reaction coordinate and was fixed during each MD simulation. A series of MD simulations were carried at different ion-separation distances for three ion pairs: acetate−$Li^+$, acetate−$Na^+$, and acetate−$K^+$. These simulations were performed with a cubic box containing the ion pair solvated with 775 water molecules. All of the simulations were performed in a NVT ensemble, with periodic boundary conditions applied in all three directions with a time step of 2 fs.[29] Long-range electrostatic interactions were handled using the Ewald summation technique, and the SHAKE algorithm was used to fix the internal geometry.[30,31]

## III. RESULTS AND DISCUSSION

We begin this discussion by presenting the structural results for an acetate anion in water and comparing them with previously reported results.[32,33] As was stated above, our acetate anion potential parameters were optimized so the computed hydration enthalpy matched the experimentally obtained enthalpy. In Figure 1a, we show radial distribution functions (RDF) for the oxygen atoms of acetate and water. In Figure 1b, we show spatial distributions (i.e., iso-density surfaces) of water around the acetate ion. The red color indicates the density of oxygen, and white color indicates the hydrogen. These iso-density surfaces correspond to 4 times the bulk density of water. Because of strong polar interactions, we observed a predominant water density around the oxygen atoms of the acetate ion. Integration of O−OW RDF up to the first minima gives 3.4 water molecules. The O−HW RDF is shifted left by 1 Å, which indicates a hydrogen bond between the water and oxygen atoms of the acetate ion. This hydrogen-bond behavior also is observed in the iso-density plot (Figure 1b). The results from our structural analysis are similar to the results reported in previous work using a nonpolarizable potential model.[34]

The main focus of this work was to use the PMF approach to quantify the solvent effect on interactions between alkali cations and the acetate anion in water. Figure 2a shows the gas-phase interactions between these ion pairs. As expected, the $Li^+$−acetate anion has a deeper minimum energy and a smaller distance as compared to the corresponding $Na^+$−acetate and $K^+$−acetate ion pairs; the reason for this difference is that $Li^+$ has a smaller ion radius and higher charge density. With the increase in ion radius, the curves shift toward the right. Figure 2b shows the corresponding computed PMFs for these three different ion pairs in water. Two significant free-energy minima are observed in the PMFs of all three of the ion pairs. The first minimum corresponds to the contact ion pair (CIP), and the second minimum corresponds to the solvent separated ion pair (SSIP). The center of mass separations between the ions in water for the CIP and SSIP states are provided in Table 2. The CIP and SSIP distances obtained from PMF for the case of $Na^+$ are very similar to the previous studies by Kirkpatrick and co-workers.[35] On physical grounds, it is clear that the existence of such minima primarily results from the balance between the ion−water and the ion−ion interactions. Similar to gas-phase interaction energy plots, we can notice a significant shift in contact ion minima of the PMFs with the increase in ion radius. One of the most important observations that can be concluded from this figure is that the depth of CIP minimum for the case of $Na^+$ is deeper than that for $Li^+$ and $K^+$. This indicates that sodium has higher CIP affinity as compared to that of $K^+$ and $Li^+$.

We computed the association constant, $K_a$, for all three ion pairs:

$$K_a = N \int_o^{r_a} 4\pi r^2 e^{-W(r)/k_bT} dr \quad (1)$$

Here, $N$ is Avogadro's number, $k_b$ is the Boltzmann constant, and $r_a$ is the ion pair separation distance at the first barrier. As is seen from Table 2, the association constant for the $Na^+$−acetate contact ion pair is higher than that for the cases of $K^+$ and $Li^+$. Both contact ion minima and the association constants indicate higher ion pair affinity for the case of $Na^+$.

The higher affinity of $Na^+$ is consistent with Collins law of matching hydration enthalpies. According to Collins law,


dx.doi.org/10.1021/jp301859z | J. Phys. Chem. B 2012, 116, 7492−7498

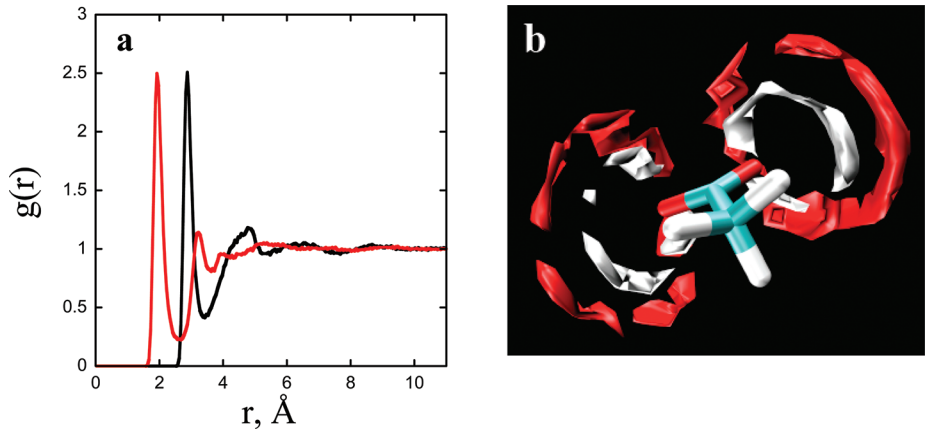


**Figure 1.** (a) Computed radial distribution functions between the oxygen atoms of acetate and oxygen (black) and hydrogen (red) atoms of water. (b) Spatial distribution of oxygen (red) and hydrogen (white) atoms of water around acetate ion. The iso-densities shown in the plot are 4 times the bulk density of water.

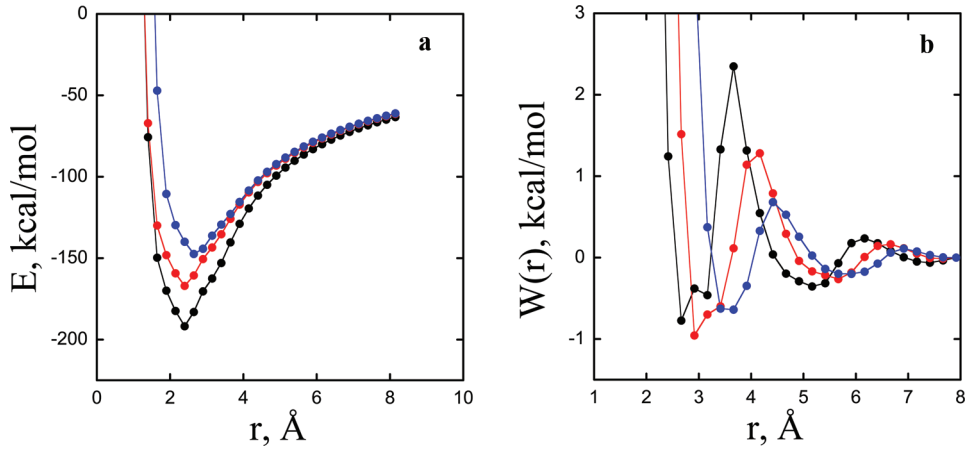


**Figure 2.** (a) Computed gas-phase interaction for different ion pairs ($Li^+$, black; $Na^+$, red; $K^+$, blue). (b) Computed corresponding potentials of mean force ($Li^+$, black; $Na^+$, red; $K^+$, blue).

**Table 2. Center of Mass Separation for CIP and SSIP for All Three Different Cases Studied**

| | CIP (Å) | SSIP (Å) |
|---|---|---|
| $Li^+$ | 2.66 | 5.16 |
| $Na^+$ | 2.92 | 5.66 |
| $K^+$ | 3.42 | 5.91 |

hydration enthalpies of ions that are very close in value correlate with higher ion-pair affinities in water.[20,21] Therefore, Collins law predicts the higher affinity for $Na^+$ in water as compared to that of $K^+$ because the hydration enthalpy of $Na^+$ is approximately equal to that of the acetate ion. In addition, when we compared the interaction energy plots (Figure 2a) in the gas phase with the PMF plots (Figure 2b) in water, we observed a significant right shift in the first minimum of the PMF for the $K^+$–acetate ion pair. This behavior can be attributed to the mobility of water and the strength of ion–water interactions around the CIP.

The results from our simulation studies, and the experimental observations by Saykally and co-workers as well as by winter and co-workers, all agree on the fact that $Na^+$ has higher affinity over $K^+$.[19,20] However the ordering of ion pair affinity for $Li^+$ with respect to $Na^+$ and $K^+$ is inconclusive from our simulation data. The well depth of the contact ion minima indicates higher affinity for $Li^+$ than for $K^+$, but the $K_a$ values indicate the higher affinity of $K^+$ than $Li^+$. Even the experiments of Saykally and co-workers do not agree with those of Winter and co-workers for the case of $Li^+$. Recent work by Murdachaew and co-workers on ion specific interactions of alkali cations with dicarboxylate dianions clearly indicates the variations in ion specificity upon changing the alkyl chain length of the dicarboxylate ion.[36] Also, Allen and co-workers through their vibrational sum frequency generation spectroscopic studies showed that $K^+$ has stronger binding affinity to the carboxylate group of the fatty acids as compared to that of $Na^+$.[37] All of these studies indicate that the ion specificity, which plays a key role in many biological processes, is system dependent and related to a fine balance between several factors like size and structure of ions, interactions between the ions, and also ion–solvent interactions.

We also evaluated the equilibrium constant, $K_{eq}$, between the CIP and SSIP pairs using eq 2.

$$K_{eq} = \frac{\int_{r_a}^{r_b} 4\pi r^2 e^{-W(r)/k_bT}\,dr}{\int_{o}^{r_a} 4\pi r^2 e^{-W(r)/k_bT}\,dr} \quad (2)$$

Here, $r_b$ is the ion pair separation distance at the second barrier. We found that $K_{eq} > 0$ for all three ion pairs, showing that equilibrium favors the SSIP over the CIP for all cases.


dx.doi.org/10.1021/jp301859z | J. Phys. Chem. B 2012, 116, 7492–7498

In Figure 3, we show the iso-density plots for CIP and SSIP states. These plots provide insight into the water structure around the ion pair along the reaction coordinate. Careful observation of the iso-density plots for the CIP clearly shows significantly higher water densities around the ion pair for the case of $Li^+$ and $Na^+$ than for $K^+$. This means that water around the CIP of $Li^+$ and $Na^+$ is more structured and less mobile, and also is evidence of a stable CIP formation for $Li^+$ and $Na^+$ when compared to that of $K^+$. In Figure 4a, we plot the computed RDFs between the cations and oxygen atoms of water at CIP distance. As expected, the intensities of first peak indicate higher water density for the case of $Li^+$ followed by $Na^+$ then by $K^+$. The coordination numbers obtained by integrating the RDFs up to the first minimum are 3.0 for $Li^+$, 3.5 for $Na^+$, and 4.5 for $K^+$. $Li^+$ has an intense first peak in the RDF as compared to $Na^+$ and $K^+$ but has a lower coordination number than the other ions, which means that the higher density for $Li^+$ indicated by the first peak of RDFs is mainly due to the smaller size of ions. In Figure 4b we also show the rotational relaxation for water in the first solvation shell (3.5 Å) of the ion pair at the CIP position of the reaction coordinate. This plot is an autocorrelation function of the angular bisector of the water molecule. The decay of the autocorrelation function is significantly faster for the case of $K^+$ when compared to $Li^+$ and $Na^+$. This means the water molecules in the first solvation shell of $K^+$ are more flexible than those of $Na^+$ or $Li^+$.

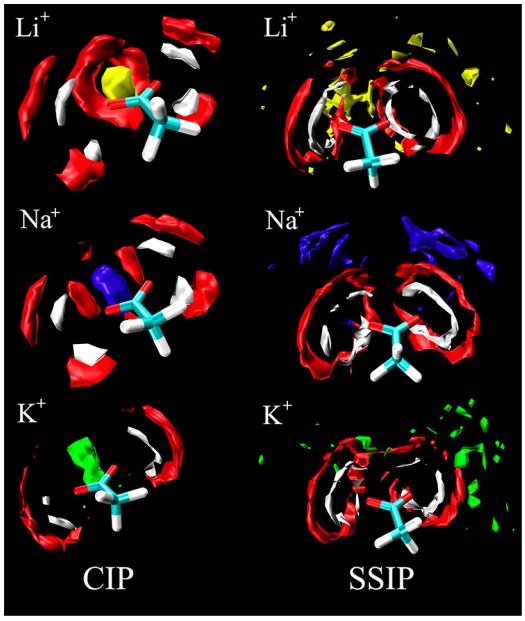


**Figure 3.** Iso-density plots for water and alkali metal ions ($Li^+$, yellow; $Na^+$, blue; $K^+$, green) around acetate. In the iso-density plots for CIP, densities represent the occupany value of 50 for 4000 frames. In SSIP case, the occupancy value is 8 for $Li^+$ and $Na^+$ and 5 for $K^+$. If the occupancy value is "*n*", it means that the particle is found at least "*n*" times in a particular grid. Iso-density of water (oxygen, red; hydrogen, white) in these plots corresponds to 4 times the bulk density of water.

We also investigated the kinetics of CIP and SSIP interconversion. According to classical transition state theory, the rate constant for CIP dissociation can be computed using eq 3. The rate for reverse reaction or the ion pair association is given by eq 4.

$$k_f^{TST} = \sqrt{\frac{k_b T}{2\pi\mu}} \frac{(r_a)^2 e^{-k_b T w(r_a)}}{\int_0^{r_a} r^2 e^{-k_b T w(r)} dr} \quad (3)$$

$$k_r^{TST} = \sqrt{\frac{k_b T}{2\pi\mu}} \frac{(r_a)^2 e^{-k_b T w(r_a)}}{\int_{r_a}^{r_m} r^2 e^{-k_b T w(r)} dr} \quad (4)$$

where $r_a$ is the position of the barrier maximum, $r_m$ is some value or $r$ representing the diffusive motion, $\mu$ is the reduced mass, $k_b$ is the Boltzmann constant, and $T$ is the temperature. The rate constants from transition state theory are shown in Table 4. The rate constants $k_f^{TST}$ and $k_r^{TST}$ are in the order of $Li^+$

**Table 3. Dissociative Barrier ($\Delta G^{\ddagger}$), Ionic Association ($K_a$), Binding Free Energy ($\Delta G$), and Equilibrium Constant ($K_{eq}$)**

| | $\Delta G^{\ddagger}$ (kcal/mol) | $K_a$ ($M^{-1}$) | $\Delta G$ (kcal/mol) | $K_{eq}$ |
|---|---|---|---|---|
| $Li^+$ | 3.12 | 0.12 | 1.24 | 4.09 |
| $Na^+$ | 2.24 | 0.23 | 0.88 | 2.53 |
| $K^+$ | 1.32 | 0.22 | 0.89 | 2.88 |

**Figure 4.** (a) Computed radial distribution function between cation and oxygen of water at the CIP position ($Li^+$, black; $Na^+$, red; $K^+$, blue). (b) Computed rotational relaxation for water in the first solvation shell (3.5 Å) of ion pair at the CIP position of reaction coordinate ($Li^+$, black; $Na^+$, red; $K^+$, blue).

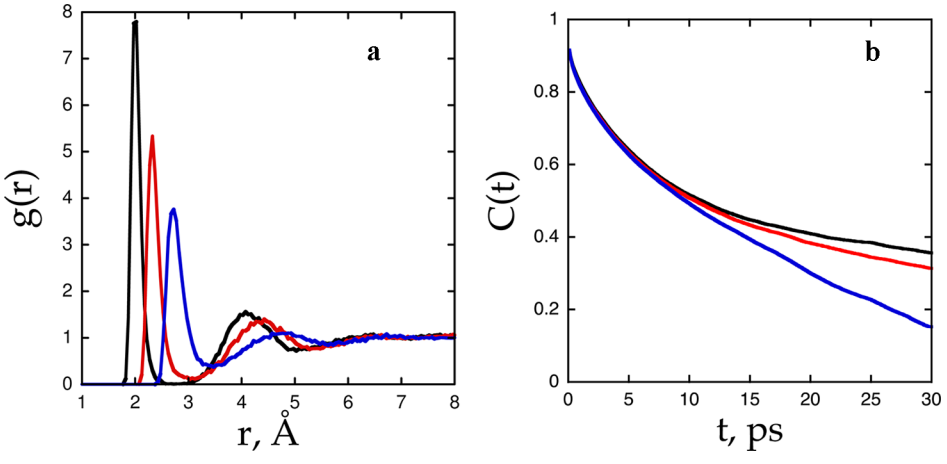



dx.doi.org/10.1021/jp301859z | J. Phys. Chem. B 2012, 116, 7492−7498

**Table 4. Results from Rate Theories**

| | $Li^+$ | $Na^+$ | $K^+$ |
|---|---|---|---|
| barrier position, $r_a$, Å | 3.66 | 4.16 | 4.41 |
| TST rate constant $k_f^{TST}$, $ps^{-1}$ for ion pair dissociation | 0.047 | 0.110 | 0.297 |
| TST rate constant $k_r^{TST}$, $ps^{-1}$ for ion pair association | 0.005 | 0.024 | 0.062 |
| barrier frequency $\omega_b$, $ps^{-1}$ | 39.01 | 16.00 | 12.03 |
| friction coefficient $\zeta$, $ps^{-1}$ | 930.33 | 1367.07 | 922.05 |
| Kramer's theory transmission coefficient $\kappa_{Kr}$ | 0.042 | 0.012 | 0.013 |
| reactive frequency, $\lambda_r$ | 17.36 | 1.46 | 0.88 |
| friction coefficient at reactive frequency $\zeta_{\lambda_r}$, $ps^{-1}$ | 70.30 | 416.54 | 328.73 |
| Grote–Hynes theory transmission coefficient $\kappa_{GH}$ | 0.445 | 0.091 | 0.073 |

< $Na^+$ < $K^+$. This can be explained on the basis of the barrier heights of the PMFs. According to the transition state theory, the rate of a reaction depends on the height of the activation barrier. The higher is the activation barrier, the slower is the rate of reaction. The dissociative barrier heights reported in Table 3 agree with this argument.

The assumption of transition state is that once the reactants reach the transition state, they will directly end up on the products side without any recrossings into the reactants. As a result, transition state theory breaks down for the reactions involving strongly interacting solvents due to the dynamical coupling between the reactive species and solvent molecules in the barrier region. These recrossings are accounted for using a transmission coefficient correction to the transition state theory. The corrected rate constant $k$ is given by $k = \kappa k^{TST}$, where $\kappa$ is the transmission coefficient that adjusts the rate constant $k^{TST}$ from transition state theory. We compute transmission coefficients using Kramer's theory[38] as well as Grote–Hynes (GH) theory.[39−41] Both of these theories use the generalized Langevin equation for the time evolution of reaction coordinate. According to Kramer's theory, the transmission coefficient $\kappa_{Kr}$ can be computed using eq 5.

$$\kappa_{Kr} = \sqrt{1 + \left(\frac{\zeta}{2\omega_b}\right)^2} - \frac{\zeta}{2\omega_b} \tag{5}$$

where $\zeta$ is a constant friction coefficient given by $\int_0^\infty \zeta(t)\, dt$. $\zeta(t)$ is the friction kernel defined by the time correlation function of the random force $(F(t,r))$ on the reaction coordinate due to the solvent, and $\omega_b$ is the barrier frequency obtained by fitting the PMF in the barrier region to an inverted parabola. The friction kernel can be computed using eq 6, where $\mu$ is the reduced mass of the ion pair.

$$\zeta(t) = \frac{1}{\mu k_b T}\langle R(t, r_a)\cdot R(0, r_a)\rangle \tag{6}$$

$$R(t, r) = F(t, r) - \langle F(t, r)\rangle \tag{7}$$

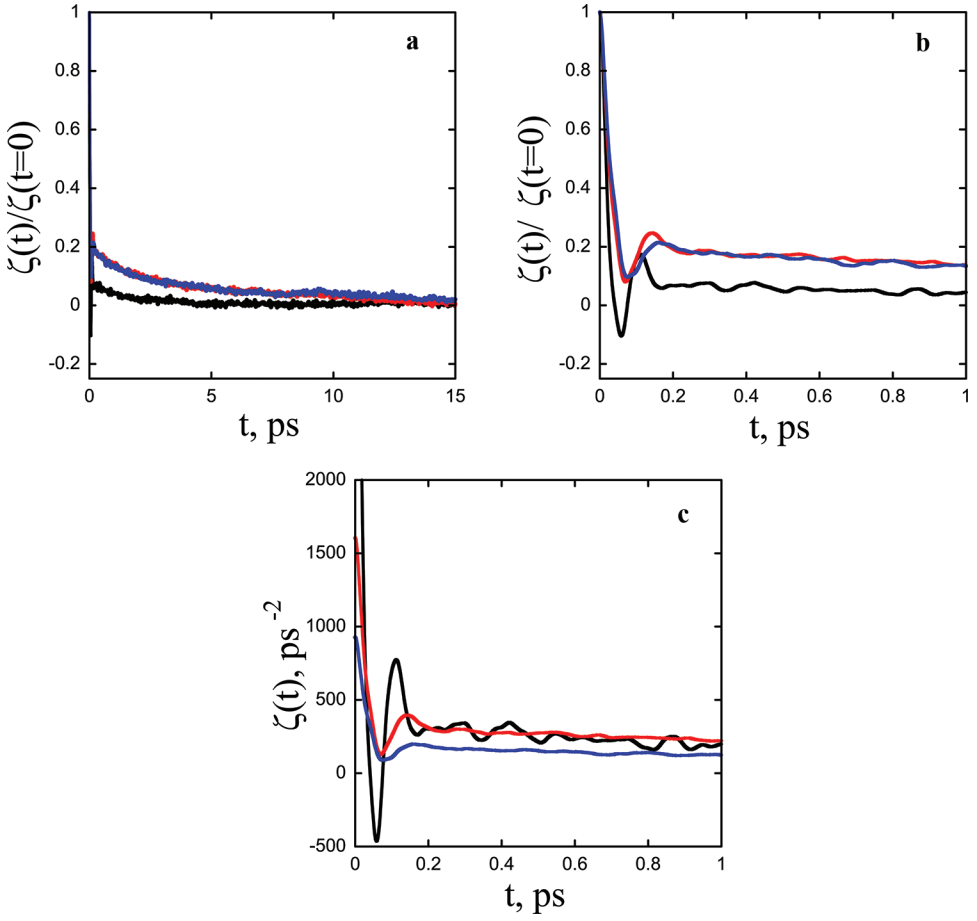


**Figure 5.** Computed friction kernels (a) normalized and plotted up to 15 ps, (b) normalized and plotted up to 1 ps, and (c) un-normalized and plotted up to 1 ps ($Li^+$, black; $Na^+$, red; $K^+$, blue).


dx.doi.org/10.1021/jp301859z | J. Phys. Chem. B 2012, 116, 7492−7498

According to GH theory, the transmission coefficient is given by $\kappa_{GH} = \lambda_r/\omega_b$, where the reactive frequency $\lambda_r$ can be computed iteratively using eq 8.

$$\lambda_r = \omega_b^2(\lambda_r + \int_0^\infty \zeta(t)e^{-\lambda_r t}dt)^{-1} \quad (8)$$

$\kappa_{GH}$ can also be expressed as

$$\kappa_{GH} = \left(\kappa_{GH} + \int_0^\infty dt\frac{\zeta(t)}{\omega_b}e^{-\omega_b\kappa_{GH}t}\right)^{-1} \quad (9)$$

The GH theory transmission coefficient involves the frequency component of the time-dependent friction coefficient $\zeta(t)$ at the Laplace frequency $\omega_b\kappa_{GH}$ relevant in the barrier region. Ignoring the time dependence of the friction coefficient in eq 9 gives the $\kappa_{GH} = \kappa_{Kr}$, which means the constant friction coefficient of Kramer's theory corresponds to zero frequency value of the time-dependent friction coefficient.

We computed the friction kernels for all three ion pairs using the trajectories at the barrier region. In Figure 5a, we show the plot of normalized friction kernels ($\zeta_N(t) = \zeta(t)/\zeta(t=0)$) up to 15 ps. For the sake of clarity in Figure 5a and b, we show the plots of friction kernels up to 1 ps. Figure 5b corresponds to un-normalized frictions kernels. In all three cases, there are two distinct time scales of decay. All of them show an initial rapid decay lasting less than 0.1 ps, followed by a long-time decay that lasts for a few picoseconds. We notice that both the short time and the long time decays are faster for the case of $Li^+$. The decay patterns for $Na^+$ and $K^+$ are very similar. It has already been shown previously that $\zeta(0)$ depends on the ionic species as well as on transition state position $r_a$.[42−44]

All of the results from the rate theory are reported in Table 4. The barrier frequency $\omega_b$ is in the order of $Li^+ > Na^+ > K^+$. This can be clearly noticed in the PMF, as the barrier for the case of $Li^+$ is much steeper when compared to $Na^+$ and $K^+$. This means that the $Li^+$−acetate ion pair spends less time around the transition state. Kramer's theory transmission coefficients $\kappa_{Kr}$ are very low for all of the ion pairs, indicating a significant role of solvent friction. The GH theory transmission coefficients $\kappa_{GH}$ are higher than the $\kappa_{Kr}$ values. This is consistent with several previous studies,[40,42−44] because Kramer's formula includes the friction due to the solvent, just as constant friction coefficient, ignoring the time dependence that is relevant with reactive motion. The $\kappa_{GH}$ value for $Li^+$ is significantly higher as compared to $Na^+$ and $K^+$. $\kappa_{GH}$ depends on the curvature of the barrier $\omega_b$ and the solvent dynamics expressed by friction kernel $\zeta(t)$ on a time scale of $\lambda^{-1}$. Since $\omega_b$ for $Li^+$ is very high, the reactive species in this case spends less time at the barrier region, and therefore effective friction due to solvent molecules is less because of the short time scale response given by the early part of time-dependent friction $\zeta(t)$. This can also be noticed in the frequency-dependent friction constants $\zeta_\lambda$ reported in Table 4.

## IV. CONCLUSION

We studied specific ion interactions between the alkali cations (i.e., $Li^+$, $Na^+$, and $K^+$) and an acetate anion in aqueous solution using MD techniques and polarizable potential models. We used these model systems to advance the understanding of the interaction between ions and protein surfaces in biological systems. We analyzed the free energy profiles for the $Li^+$/ $Na^+$/ $K^+$−acetate ion-pairs. The values of contact ion minima and the association constants both indicate higher affinity for the $Na^+$−acetate ion pair than the corresponding $K^+$−acetate pair. This observation is in agreement with the experimental XAS measurements. The ordering of $Li^+$−acetate pair with respect to $Na^+$ and $K^+$ remains inconclusive. Through our structural analysis, we provide insight on water structuring around the ion pair along the reaction coordinate. Our spatial distributions indicate strong water structuring around the CIP of $Na^+$ and $Li^+$. We also studied the kinetics of ion pair interconversion. Our results indicate that the transition state theory rate constants are in the order of $K^+ > Na^+ > Li^+$, which follows the barrier heights, but the GH transmission coefficients are in the order of $Li^+ > Na^+ > K^+$. This is because the GH theory transmission coefficients are very sensitive to the barrier frequency. The steeper is the barrier curvature, the shorter is the time spent by the reactive species at the transition state, and hence solvent has less time to influence the barrier crossing events.

## AUTHOR INFORMATION

### Corresponding Author

*E-mail: liem.dang@pnl.gov.

### Notes

The authors declare no competing financial interest.

## ACKNOWLEDGMENTS

This work was supported by the U.S. Department of Energy (DOE), Office of Basic Energy Sciences (BES), Division of Chemical Sciences, Geosciences and Biosciences. Pacific Northwest National Laboratory is a multiprogram national laboratory operated for DOE by Battelle. The calculations were carried out using computer resources provided by BES.

## REFERENCES

(1) Perez-Jimenez, R.; Godoy-Ruiz, R.; Ibarra-Molero, B.; Sanchez-Ruiz, J. M. *Biophys. J.* **2004**, *86*, 2414−2429.
(2) Zhang, Y. J.; Furyk, S.; Bergbreiter, D. E.; Cremer, P. S. *J. Am. Chem. Soc.* **2005**, *127*, 14505−14570.
(3) Bostrom, M.; Williams, D. R. M.; Ninham, B. W. *Langmuir* **2001**, *17*, 4475−4478.
(4) Kunz, W.; Lo Nostro, P.; Ninham, B. W. *Curr. Opin. Colloid Interface Sci.* **2004**, *9*, 1−18.
(5) Collins, K. D. *Methods* **2004**, *34*, 300−311.
(6) Nostro, P. L.; Ninham, B. W. *Chem. Rev.* **2012**, *112*, 2286−2322.
(7) Vrbka, L.; Jungwirth, P.; Bauduin, P.; Touraud, D.; Kunz, W. *J. Phys. Chem. B* **2006**, *110*, 7036−7043.
(8) Lund, M.; Vrbka, L.; Jungwirth, P. *J. Am. Chem. Soc.* **2008**, *130*, 11582−11583.
(9) Jungwirth, P.; Tobias, D. J. *Chem. Rev.* **2006**, *106*, 1259−1281.
(10) Hess, B.; van der Vegt, N. F. A. *Proc. Natl. Acad. Sci. U.S.A.* **2009**, *106*, 13296−13300.
(11) Hofmiester, F. *Arch. Exp. Pathol. Pharmakol.* **1888**, *24*, 247−260.
(12) Omta, A. W.; Kropman, M. F.; Woutersen, S.; Bakker, H. J. *Science* **2003**, *301*, 347−349.
(13) Kropman, M. F.; Bakker, H. J. *J. Am. Chem. Soc.* **2004**, *126*, 9135−9141.
(14) Kropman, M. F.; Bakker, H. J. *Science* **2001**, *291*, 2118−2120.
(15) Kropman, M. F.; Bakker, H. J. *J. Chem. Phys.* **2001**, *115*, 8942−8948.
(16) Batchelor, J. D.; Olteanu, A.; Tripathy, A.; Pielak, G. J. *J. Am. Chem. Soc.* **2004**, *126*, 1958−1961.
(17) Smith, J. D.; Saykally, R. J.; Geissler, P. L. *J. Am. Chem. Soc.* **2007**, *129*, 13847−13856.
(18) Vrbka, L.; Vondrášek, J.; Jagoda-Cwiklik, B.; Vácha, R.; Jungwirth, P. *Proc. Natl. Acad. Sci. U.S.A.* **2006**, *103*, 15440−15444.

(19) Uejio, J. S.; Schwartz, C. P.; Duffin, A. M.; Drisdell, W. S.; Cohen, R. C.; Saykally, R. J. *Proc. Natl. Acad. Sci. U.S.A.* **2008**, *105*, 6809−6812.
(20) Aziz, E. F.; Ottosson, N.; Eisebitt, S.; Eberhardt, W.; Jagoda-Cwiklik, B.; Vácha, R.; Jungwirth, P.; Winter, B. *J. Phys. Chem. B* **2008**, *112*, 12567−12570.
(21) Dang, L. X.; Chang, T. M. *J. Chem. Phys.* **1997**, *106*, 8149−8159.
(22) Wang, J. M.; Wang, W.; Kollman, P. A.; Case, D. A. *J. Mol. Graphics Modell.* **2006**, *25*, 247−260.
(23) Wang, J. M.; Wolf, R. M.; Caldwell, J. W.; Kollman, P. A.; Case, D. A. *J. Comput. Chem.* **2004**, *25*, 1157−1174.
(24) Frisch, M. J.; Trucks, G. W.; Schlegel, H. B.; Scuseria, G. E.; Robb, M. A.; Cheeseman, J. R.; Zakrzewski, V. G.; Montgomery, J. A., Jr.; Stratmann, R. E.; Burant, J. C.; et al. *Gaussian 98*, revision A.6; Gaussian, Inc.: Pittsburgh, PA, 1998.
(25) Case, D. A.; Darden, T. A.; Cheatham, T. E., III; Simmerling, C. L.; Wang, J.; Duke, R. E.; Luo, R.; Merz, K. M.; Pearlman, D. A.; Crowley, M.; et al. *Amber 9*; University of California: San Francisco, CA, 2006.
(26) Marcus, Y. *Biophys. Chem.* **1994**, *51*, 111−118.
(27) Guardia, E.; Rey, R.; Padro, J. A. *Chem. Phys.* **1991**, *155*, 187−195.
(28) Ciccotti, G.; Ferrario, M.; Hynes, J. T.; Kapral, R. *Chem. Phys.* **1989**, *129*, 241−251.
(29) Ryckaert, J. P.; Ciccotti, G.; Berendsen, H. J. C. *J. Comput. Phys.* **1977**, *23*, 327−341.
(30) Berendsen, H. J. C.; Postma, J. P. M.; Vangunsteren, W. F.; Dinola, A.; Haak, J. R. *J. Chem. Phys.* **1984**, *81*, 3684−3691.
(31) Essmann, U.; Perera, L.; Berkowitz, M. L.; Darden, T.; Lee, H.; Pedersen, L. G. *J. Chem. Phys.* **1995**, *103*, 8577−8594.
(32) Jorgensen, W. L.; Gao, J. *J. Phys. Chem.* **1986**, *90*, 2174−2182.
(33) Gao, J.; Garner, D. S.; Jorgensen, W. L. *J. Am. Chem. Soc.* **1986**, *108*, 4784−4790.
(34) Meng, E. C.; Kollman, P. A. *J. Phys. Chem.* **1996**, *100*, 11460−11470.
(35) Iskrenova-Tchoukova, E.; Kalinichev, A. G.; Kirkpatrick, R. J. *Langmuir* **2010**, *26*, 15909−15919.
(36) Murdachaew, G.; Valiev, M.; Kathmann, S. M.; Wang, X. B. *J. Phys. Chem. A* **2012**, *116*, 2055−2061.
(37) Tang, C. Y.; Allen, H. C. *J. Phys. Chem. A* **2009**, *113*, 7383−7393.
(38) Kramers, H. A. *Physica* **1940**, *7*, 284−304.
(39) Grote, R. F.; Hynes, J. T. *J. Chem. Phys.* **1980**, *73*, 2715−2733.
(40) Ciccotti, G.; Ferrario, M.; Hynes, J. T.; Kapral, R. *J. Chem. Phys.* **1990**, *93*, 7137−7147.
(41) Gertner, B. J.; Wilson, K. R.; Zichi, D. A.; Lee, S.; Hynes, J. T. *Faraday Discuss.* **1988**, *85*, 297−308.
(42) Das, A. K.; Madhusoodanan, M.; Tembe, B. L. *J. Phys. Chem. A* **1997**, *101*, 2862−2872.
(43) Sese, G.; Guardia, E.; Padro, J. A. *J. Phys. Chem.* **1995**, *99*, 12647−12654.
(44) Rey, R.; Guardia, E.; Padro, J. A. *J. Chem. Phys.* **1992**, *97*, 1343−1352.